THE JOURNAL OF BIOLOGICAL CHEMISTRY
Vol. 279, No. 30, Issue of July 23, pp. 31780–31787, 2004
Printed in U.S.A.

Quantitative NAD(P)H/Flavoprotein Autofluorescence Imaging Reveals Metabolic Mechanisms of Pancreatic Islet Pyruvate Response*

Received for publication, December 22, 2003, and in revised form, April 26, 2004
Published, JBC Papers in Press, May 17, 2004, DOI 10.1074/jbc.M314005200

Jonathan V. Rocheleau, W. Steven Head, and David W. Piston‡

From the Molecular Physiology and Biophysics, Vanderbilt University, Nashville, Tennessee 37232

Glucose-stimulated insulin secretion is a multistep process dependent on β-cell metabolic flux. Our previous studies on intact pancreatic islets used two-photon NAD(P)H imaging as a quantitative measure of the combined redox signal from NADH and NADPH (referred to as NAD(P)H). These studies showed that pyruvate, a non-secretagogue, enters β-cells and causes a transient rise in NAD(P)H. To further characterize the metabolic fate of pyruvate, we have now developed one-photon flavoprotein microscopy as a simultaneous assay of lipoamide dehydrogenase (LipDH) autofluorescence. This flavoprotein is in direct equilibrium with mitochondrial NADH. Hence, a comparison of LipDH and NAD(P)H autofluorescence provides a method to distinguish the production of NADH, NADPH, or both. Using this method, the glucose dose response is consistent with an increase in both NADH and NADPH. In contrast, the transient rise in NAD(P)H observed with pyruvate stimulation is not accompanied by a significant change in LipDH, which indicates that pyruvate raises cellular NADPH without raising NADH. In comparison, methyl pyruvate stimulated a robust NADH and NADPH response. These data provide new evidence that exogenous pyruvate does not induce a significant rise in mitochondrial NADH. This inability likely results in its failure to produce the ATP necessary for stimulated secretion of insulin. Overall, these data are consistent with either a restricted pyruvate dehydrogenase-dependent metabolism or a buffering of the NADH response by other metabolic mechanisms.

The redox potential of β-cells increases in response to a rise in extracellular glucose. This redox response can be assayed using two-photon excitation NAD(P)H microscopy (1–3). This method provides excellent spatial and temporal resolution of the nutrient-stimulated NAD(P)H response but makes no distinction between NADH and NADPH (1). The NADH generated during glucose stimulation transfers its reducing power to the electron transport chain (ETC),[1] resulting in ATP-dependent insulin secretion (4). The NADPH generated has been proposed to modulate the ATP-dependent response directly (5) and provide information on the build-up of tricarboxylic acid cycle intermediates that modulate the ATP-dependent response (6, 7). In contrast to glucose, exogenous pyruvate causes a small transient NAD(P)H response (3) and does not cause insulin secretion in the absence of other signals (4). Separately measuring the pyruvate-stimulated NADH and NADPH responses will provide insight into the inability of this metabolite to cause insulin secretion.

Pyruvate produced from glycolysis enters β-cell mitochondrial metabolism nearly equally through pyruvate dehydrogenase (PDH) and pyruvate carboxylase (PC) (8–11). PDH metabolism generates acetyl-CoA to produce NADH in the tricarboxylic acid cycle, supporting ATP-dependent insulin secretion (4). PC-dependent metabolism increases tricarboxylic acid cycle intermediates (10, 12), which stimulates proportional NADPH production through pyruvate and citrate cycling as well as through isocitrate dehydrogenase (13). NADPH can be produced via cytoplasmic or mitochondrial isocitrate dehydrogenase. A cycle is formed when isocitrate exits the mitochondrial matrix and is converted to α-ketoglutarate, which can then re-enter the mitochondrial matrix. The tricarboxylic acid cycle intermediates and the NADPH produced likely modulate the ATP-dependent response because PC activity correlates directly with insulin secretion (11). Tricarboxylic acid cycle intermediates are proposed to modulate the ATP-dependent response through the production of long chain acyl-CoA and other signaling molecules (6, 7). The NADPH produced is proposed to directly modulate the ATP-dependent pathway by acting as a substrate for nitric-oxide synthase and glutathione reductase (5). Regardless of the specific action of NADPH, its levels report on the "ATP-independent pathway" of insulin (4). Therefore, an assay of NADH and NADPH provides evidence for the metabolic fate of pyruvate and a measure of the ATP-dependent and -independent mechanisms of insulin secretion.

Another source of redox related autofluorescence comes from cellular flavins (14, 15). Like NAD(P)H, flavins show differential fluorescence between their oxidized and reduced states. In contrast to NAD(P)H, these molecules are fluorescent in their oxidized state. A significant fraction of flavin-associated autofluorescence is nonredox-responsive, resulting in significant nonresponsive intensity. A large contributor to this nonresponsive intensity is free flavins, because their oxidation state is not directly coupled to the electron transport chain. Flavins are generally quenched when bound as protein cofactors (17, 18). As a result of this quenching, the majority of flavoproteins contribute little to the autofluorescence intensity.

* This work was supported through National Institutes of Health Grant DK53434, National Science Foundation Grant DBI9871063 (to D. W. P.), and individual National Institutes of Health National Research Science Award DK59737 (to J. V. R.). The costs of publication of this article were defrayed in part by the payment of page charges. This article must therefore be hereby marked "*advertisement*" in accordance with 18 U.S.C. Section 1734 solely to indicate this fact.

‡ To whom correspondence should be addressed: Molecular Physiology and Biophysics, 702 Light Hall, Vanderbilt University, Nashville, TN 37232. Tel.: 615-322-7030; Fax: 615-322-7236; E-mail: David.Piston@vanderbilt.edu.

[1] The abbreviations used are: ETC, electron transport chain; PDH, pyruvate dehydrogenase; PC, pyruvate carboxylase; LipDH, lipoamide dehydrogenase; ETF, electron transfer flavoprotein; FCCP, cyanide *p*-trifluoromethoxy-phenyl hydrazone.

Two flavoproteins that demonstrate significant redox-dependent changes in intensity are mitochondrial lipoamide dehydrogenase (LipDH) and electron transfer flavoprotein (ETF) (14, 15). The redox state of LipDH is in direct equilibrium with the mitochondrial [NADH]:[NAD^+] ratio, so as mitochondrial NADH intensity rises, LipDH intensity falls. This equilibrium allows a distinction to be made between the nutrient-stimulated NADH and NADPH responses by comparison of NAD(P)H and LipDH autofluorescence. The NAD(P)H response is due to the combined NADH and NADPH responses in the cytoplasm and mitochondria. Because of this combined response, the cellular NADPH response cannot be simply calculated from the NAD(P)H and LipDH responses. However, a rise in NAD(P)H without a change in LipDH indicates a NADPH response rather than NADH. Studies have used the red-shifted absorbance and emission of LipDH to isolate its fluorescence from that of ETF (17–20). However, significant spectral overlap of LipDH and ETF results in mixed detection. Furthermore, the LipDH and ETF redox-dependent responses need to be characterized in pancreatic islets, and the contributions from other flavins and fluorophores need to be assessed. We show that a ratio of dual color confocal microscopy (488 and 458 nm) can be used to successfully isolate the LipDH response for independent comparison with the NAD(P)H response.

Two-photon flavoprotein imaging has proven difficult (21), so we developed quasi-simultaneous imaging of flavoproteins by confocal and NAD(P)H by two-photon imaging. We first confirm that the majority of flavin redox response in this tissue is due to LipDH and ETF. We also show that the LipDH response can be isolated from that of ETF by using a fluorescence ratio of excitation wavelengths (458:488 nm). Using this multicolor autofluorescence imaging method, we demonstrate that glucose stimulation results in concomitant production of NADH and NADPH. In contrast, pyruvate stimulates a transient rise of NADPH in the absence of a significant NADH response. These experiments provide evidence that exogenous pyruvate enters cycling routes to produce NADPH, but is unable to stimulate a significant metabolic NADH response, and thus does not elicit insulin secretion.

EXPERIMENTAL PROCEDURES

Materials

Alcohol dehydrogenase (Baker's yeast), β-hydroxybutyrate, glucose, pyruvate, methyl pyruvate, rotenone, sodium cyanide, FAD, cyanide *p*-trifluoromethoxy-phenyl hydrazone (FCCP), LipDH, NADH, and mannoheptulose were all purchased from Sigma-Aldrich. Hanks' balanced salt solution and RPMI 1640 medium were purchased from Invitrogen. MitoTracker Green FM and LysoTracker Green were purchased from Molecular Probes (Eugene, OR).

Islet Isolation

Islets were extracted from 6–12-week-old C57BL/6 male mice by collagenase (Roche Applied Science) digestion (22, 23). The isolated islets were placed on human extracellular matrix (BD PharMingen, San Diego, CA) coated 35-mm glass-bottomed dishes (MatTek Corp.) as previously described (24). After ~14 days the cell matrix promotes spreading, and the islets flatten in appearance. These islets have been shown to exhibit normal glucose-stimulated NAD(P)H and insulin secretion (2, 25). Prior to experiments, these islets were equilibrated in imaging buffer (125 mM NaCl, 5.7 mM KCl, 2.5 mM $CaCl_2$, 1.2 mM $MgCl_2$, 10 mM HEPES, and 0.1% bovine serum albumin, pH 7.4) containing 2 mM glucose for 30–60 min at 37 °C under 5% CO_2. Further treatments were added as indicated.

Two-photon and Confocal Fluorescence Imaging

Two-photon and confocal imaging was done using a LSM510 laser scanning microscope with a Plan-Apochromat 63× 1.4 NA oil immersion lens (Carl Zeiss Inc., Thorwood, NY). The islets were kept at 37 °C using a temperature controlled stage and objective warmer (Zeiss Inc., Thorwood, NY).

Autofluorescence Imaging—Sequential images of autofluorescence were collected using 710- (two-photon), 458-, and 488-nm excitation. Each was collected with a single slow speed scan (6.4 μs/pixel) at 0.29 μm/pixel. Two-photon imaging of NAD(P)H used a Coherent Mira laser tuned to 710 nm (Coherent Inc., Santa Clara, CA). The laser power used provided ~3.5 mW to the surface; at this laser power no observable damage is caused to the islet (1) even after 60 min of continuous imaging (24). Nondescanned NAD(P)H fluorescence was collected through a custom 380–550-nm filter (Chroma Inc., Rockingham, VT). To limit exposure to single photon excitation, the islet regions were first brought into focus using two-photon excitation (fluorescence and differential interference contrast). Single photon confocal imaging was used only during data collection. Confocal imaging was done using the 458-nm laser line (~3 μW at sample) and a long pass 475 emission filter or the 488-nm laser line (~2.5 μW at sample) and a long pass 505 emission filter or the 543-nm laser line and a long pass 560 emission filter. The gain was set so that the bright nonresponding regions were at or near detector saturation, and this level was maintained throughout all experiments. The offset values for the 710-, 458-, and 488-nm channels were set to achieve a zero intensity intercept using standard curves of NADH, FAD, and LipDH in solution (26). These settings were monitored routinely.

Spectra Imaging—Emission spectra generated from 458-nm excitation were measured using the META detector of the LSM510 microscope (Zeiss Inc., Thorwood, NY). Regions of interest were outlined using the LSM 510 Image Browser software (version 3.6). The data were extracted from five bright nonresponsive regions, five dim responsive regions, and one larger background region in each image. The background region was used for spectral correction. The treatments were carried out on five separate islets, and each separate islet provided spectra for the bright and dimmer fluorescence regions.

Subcellular Markers—Living pancreatic islets were labeled with 30 nM MitoTraker Green FM at 37 °C for 30 min or 75 nM LysoTracker Green at 37 °C for 1 h. The islets were washed with imaging buffer. Image collection was done using sequential excitation with the 488 nm laser line with a band pass 500–530-nm emission filter and a 543-nm laser with a long pass 560 emission filter. Sequential image collection was used to minimize bleed through of the bright green fluorophores into the dimmer 543-nm excited autofluorescence.

Reduction of LipDH and ETF Flavoproteins

The data for Figs. 3 and 4 were collected using pharmacological treatments that successively reduced LipDH and ETF (14–19). Reduction of these ETC-linked flavoproteins quenches their autofluorescence, which allows assignment of the maximum intensity changes associated with each protein. The islets were initially placed at low redox potential in 2 mM glucose resulting in maximum LipDH and ETF intensities. After image collection, rotenone (10 μM) and β-hydroxybutyrate (10 mM) were incubated with the islets for 5 min. This treatment raised mitochondrial NADH by inhibiting the ETC at complex I (rotenone) while introducing a NADH producing metabolite (β-hydroxybutyrate). The resulting rise in mitochondrial NADH reduces LipDH fluorescence intensity (14, 15). The change in intensity after rotenone and β-hydroxybutyrate treatment is associated with the quenching of LipDH. Finally, a stock solution was added to achieve a final concentration of 3 mM cyanide and 10 mM glucose. This treatment was incubated with the islet for 5 min prior to image collection inhibiting the final step of the ETC (complex III). Inhibition of complex III reduces ETF causing a decrease in its fluorescence intensity. The change in intensity after cyanide and glucose treatment is associated with the quenching of ETF.

Fluorophore Standard Curves

Determination of the NAD(P)H and flavin concentrations was performed by imaging of standard solutions in deep well slides. FAD was imaged in Hanks' balanced salt solution buffer at 0, 13.5, 26.9, 53.9, and 108 μM. Stock FAD concentration was determined through absorbance at 450 nm, $\epsilon = 11{,}300\ M^{-1}\ cm^{-1}$. LipDH was imaged in Hanks' balanced salt solution buffer at 0, 1.2, 2.3, 4.6, 9.3, and 18.6 μM. Stock LipDH concentration was determined by absorbance at 455 nm, $\epsilon = 11{,}300\ M^{-1}\ cm^{-1}$. The absorbance ratio of 273 to 455 nm for the LipDH solution was close to 5.3, which indicates a 1:1 ratio of FAD to LipDH (27). The NAD(P)H standard curve was done with NADH bound to alcohol dehydrogenase. This solution closely resembles cellular NAD(P)H because a majority of cellular NAD(P)H is enzyme bound in the cellular environment (28). NADH was titrated into a solution of ~100 mg/ml alcohol dehydrogenase, 10 mM ethanol, 100 mM isobutyramide, 6 mM semicarbazide, and 10 mM HEPES (pH 9.0). These enzyme-bound NADH solutions were imaged at 50, 100, 200, 300, 400, 500, 600, 800, 1000, 1200, 1400, 1600, 1800, and 2500 μM.

Image Analysis

The images were exported in tagged image file format (tiff) for analysis using MetaMorph software (version 5.0). The images were filtered using a 3 × 3 median filter. An intensity threshold was set on the median filtered image. The low end of this threshold was adjusted to exclude nuclear regions, and the high end was set to partially exclude the very bright nonresponsive regions. A binary mask was made from the threshold. This mask was then eroded and dilated to remove noise pixels in the background regions. Image math using the final binary mask against the median filtered image allowed selection of our defined region for calculation of average autofluorescence intensity.

RESULTS

Characterization of Pancreatic Islet Autofluorescence—To correctly assign the intensity changes associated with flavoproteins, the contribution from other autofluorescence sources, such as lipofuscin deposits, needed to be established. Flavins are excited with either 458- or 488-nm excitation, away from the maximum excitations of tryptophan (~300 nm) and porphoryins (~400 nm) (16). The images were collected from living pancreatic islets using a wide range of excitations (Fig. 1). These images were collected with four sequential scans using the 710- (two-photon excitation; Fig. 1, *A* and *B*), 458- (Fig. 1, *C* and *D*), 488- (Fig. 1, *E* and *F*), and 543-nm (Fig. 1, *G* and *H*) laser lines. The left (Fig. 1, *A*, *C*, *E*, and *G*) and right (Fig. 1, *B*, *D*, *F*, and *H*) images were collected from the islet in buffer containing low (2 mM) and high (20 mM) glucose concentrations, respectively. These images demonstrate the type of autofluorescence generated by a wide range of excitation. NAD(P)H is the main autofluorescent fluorophore observed using two-photon 710-nm excitation and 380–550-nm emission collection (1, 24) (Fig. 1, *A* and *B*). These images demonstrate dark nuclear regions as well as bright regions dispersed over a relatively diffuse fluorescence. The bright regions correspond to mitochondria, which have a higher NAD(P)H concentration than the cytoplasmic regions (2, 28). This results in the mitochondrial NAD(P)H signal dominating the measured response. As expected, there was a significant rise in NAD(P)H fluorescence (~2-fold) with increased extracellular glucose (Fig. 1, *A* and *B*). Like 710-nm two-photon excitation, the 458- and 488-nm generated images have large dark regions corresponding to individual nuclei, as well as bright regions dispersed over dimmer fluorescence (Fig. 1, *C–F*). Absent from these images is any significant membrane intensity, which indicates minimal contribution from plasma membrane-bound flavoproteins such as NADPH oxidase. As expected for flavin fluorescence (and opposite of the NAD(P)H response), the image intensity fell as glucose was raised. However, in both the 458- and 488-nm images, the brightest regions were nonresponsive to this change in cellular redox potential. In contrast, the dim regions decrease in intensity. This dim population does not contain any definable subregions that change differentially upon glucose stimulation. The 543-nm excited images demonstrate a spotted fluorescence that did not perceivably change with glucose addition (Fig. 1, *G* and *H*). The brightest regions in these 543-nm images overlap significantly with the bright redox-nonresponsive regions of the 458- and 488-nm images (Observe the yellow overlap in Fig. 1*I* and J). These data indicate that the autofluorescence from living pancreatic islets demonstrate intensity changes consistent with flavoproteins. However, a number of bright subcellular regions are redox-nonresponsive and scattered throughout the cytoplasm.

Mitochondrial and lysozomal subcellular markers were used to further characterize the redox-nonresponsive regions of this tissue (Fig. 2). The 543-nm generated image was used to compare the nonresponsive regions (Fig. 2, *C* and *D*) with mitochondrial (Fig. 2*E*) or lysozomal (Fig. 2*F*) subcellular markers. Little overlap was observed between the nonresponsive regions

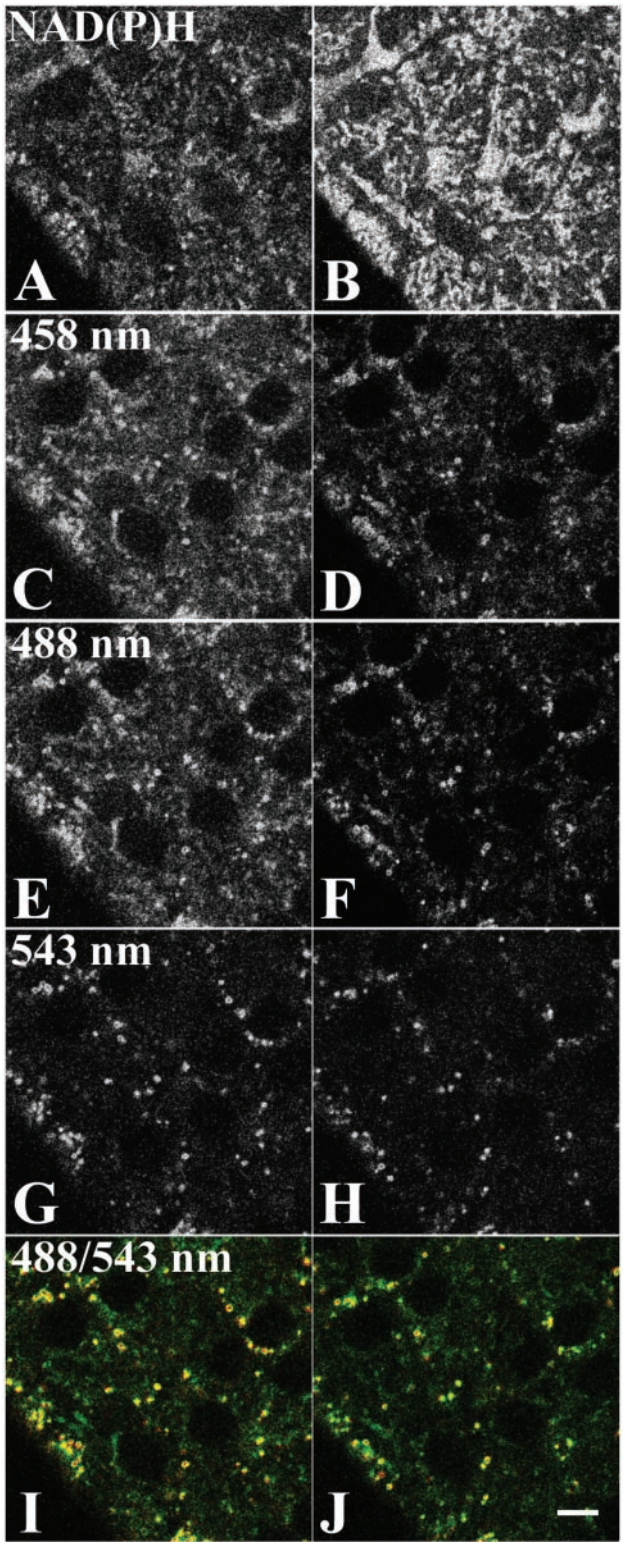

FIG. 1. **Autofluorescence collected from living pancreatic islets at low and high redox potential.** Autofluorescence generated using 710-nm (two-photon) (*A* and *B*), 458-nm (*C* and *D*), 488-nm (*E* and *F*), and 543-nm (*G* and *H*) excitation. The images in the *left panels* were collected from an islet equilibrated in imaging buffer containing 2 mM glucose (*A*, *C*, *E*, and *G*). The images in the *right panels* were collected from the same region of the islet after 5 min of exposure to 20 mM glucose (*B*, *D*, *F*, and *H*). The pseudo-color overlap of the 488 nm (*green*) and 543 nm (*red*) excited images is shown to demonstrate colocalization of the bright nonresponsive regions in both images (*I* and *J*). The *bar* shows 20 μm.

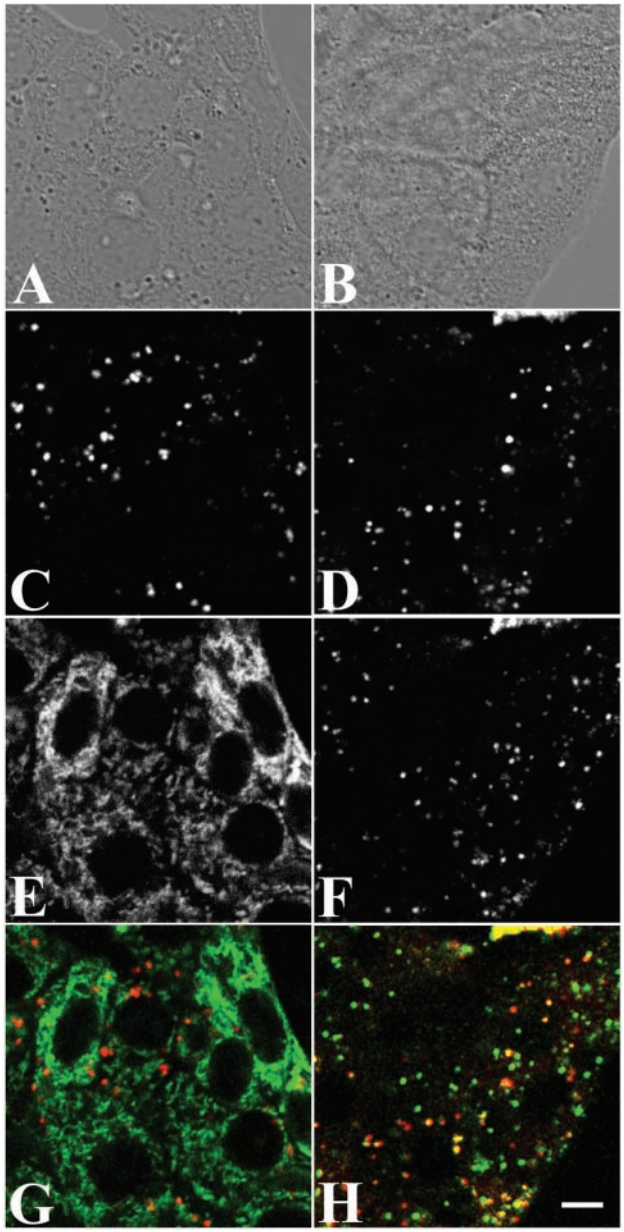

FIG. 2. **Colocalization of the redox-nonresponsive regions (lipofuscin) with mitochondrial and lysozomal subcellular markers.** The islets were labeled with either MitoTracker Green-AM or LysoTracker Green-AM. (*A* and *B*) differential interference contrast images. *C* and *D*, 543-nm excited autofluorescence to mark the redox-nonresponsive regions. The pseudo-color overlap of the Mitochondrial or Lysozomal (*green*) image with the 543-nm excited autofluorescence (*red*) is shown. *E*, MitoTracker Green-AM dye labeled image. *F*, LysoTracker Green-AM dye image. The *bar* shows 20 μm.

and the mitochondrial dye, consistent with this fluorescence not originating from mitochondrial flavoproteins (Fig. 2, compare *C* and *E* and overlap in *G*). In contrast, significant overlap was observed between the nonresponsive regions and a lysozomal cellular marker (Fig. 2, compare *D* and *F* and overlap in *H*). These data indicate that the redox-nonresponsive intensity originates from acidic vesicles rather than from mitochondria.

To further characterize the autofluorescence gathered from this tissue, images were collected of living pancreatic islets using 458-nm excitation and spectral detection (Fig. 3). This method provides both spectral and spatial resolution, which allows separate analysis of the redox-responsive and -nonresponsive regions. Shown in Fig. 3*A* are the normalized spectra of the bright nonresponsive regions and the dimmer responsive

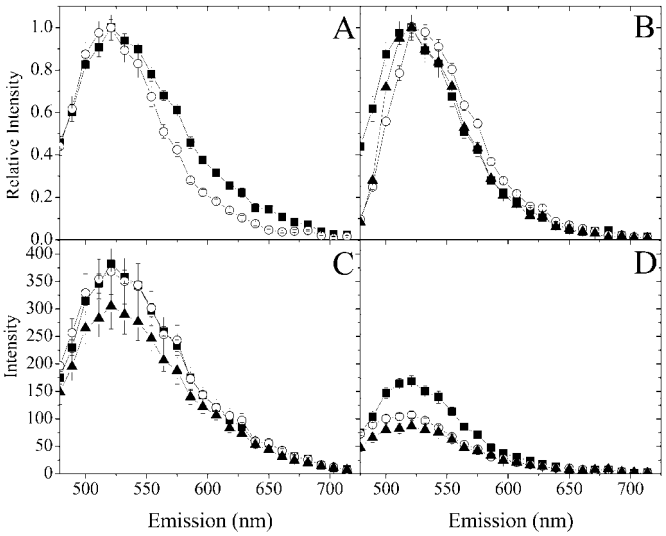

FIG. 3. **Spectral imaging of living pancreatic islet autofluorescence using 458-nm excitation.** The images were collected using 458-nm illumination and the Meta detector of an LSM510 microscope. *A*, comparison of the normalized spectra of the bright nonresponsive regions (■) to the dim redox-responsive regions (○) at 2 mM glucose. *B*, comparison of the dim redox-responsive regions spectrum (■) to FAD (○) and LipDH (▲) in solution. *C* and *D*, background corrected spectra of the bright redox-nonresponsive regions (*C*) and dim redox-responsive regions (*D*) with 2 mM glucose (■), LipDH reduction treatment (○, 2 μM rotenone + 10 mM β-hydroxybutyrate), and ETF reduction treatment (▲, 3 mM cyanide + 10 mM glucose). The data are reported as the means ± S.E. of the mean (n = 5 islets).

cellular regions. The bright nonresponsive regions have a broader red shoulder (525–620 nm) than the responsive regions. Therefore, these bright nonresponsive regions are broadly excited, overlap significantly with acidic vesicles, and have a broader red emission shoulder than the redox-responsive regions. These characteristics are consistent with lipofuscin deposits that accumulate with age in postmitotic cells (29). Because these deposits are spotted and significantly bright, they were relatively easy to avoid during analysis of the redox-responsive regions.

Spectral imaging was used to further examine the fluorescence from the redox-responsive regions of the cell. In comparison with LipDH and FAD in solution, the redox-responsive regions have a broader blue side of the spectra (Fig. 3*B*). This broadening is not due to scatter of the 458-nm excitation light in the cellular environment because the separation between cellular and solution fluorescence does not rise from 492 to 478 nm. Thus it is likely that this blue shifting is from ETF fluorescence, a component of mitochondrial flavoprotein fluorescence. The red side of all these spectra is similar, consistent with this cellular fluorescence coming from flavins.

To examine the contribution of LipDH and ETF to the cellular fluorescence, we used treatments to successively quench these proteins (Fig. 3, *C* and *D*). The changes in spectra caused by these treatments are then compared with the known or measured spectra of LipDH, ETF, and free flavins. The bright spotted regions were nonresponsive to both of these treatments (Fig. 3*C*). In contrast, significant changes occurred in the dim regions (Fig. 3*D*). The intensity dropped in the range of 500–580 nm after the reduction of LipDH (■ *versus* ○), consistent with the measured spectra of this flavoprotein. There was a small but significant drop in intensity from 479 to 530 nm after ETF reduction (○ *versus* ▲), consistent with the blue shifted emission spectra of this flavoprotein (30). A significant amount of fluorescence remains after both of these treatments, which likely originates from free flavins (14–18). Therefore, the redox

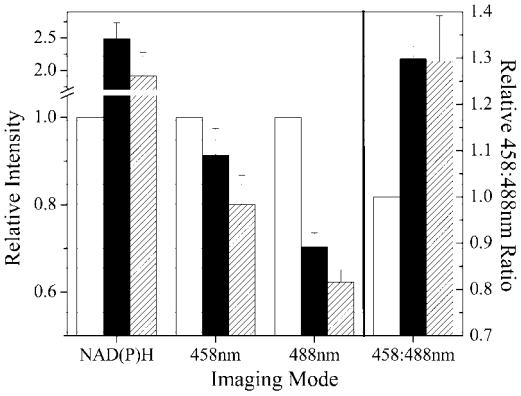

FIG. 4. **Relative changes in pancreatic islet autofluorescence to LipDH and ETF reduction.** The images were collected using 710- (two-photon), 458-, and 488-nm excitation. The islets were equilibrated in imaging buffer with 2 mM glucose (*open bars*) before reduction of LipDH (*black bars*) and ETF (*hatched bars*). *Left axis*, the changes in intensity are reported relative to the fluorescence observed in 2 mM glucose. A break in the *y* axis at 1.4 units is introduced to better examine the changes in the 458- and 488-nm fluorescence. *Right axis*, relative changes in the 458:488-nm intensity ratio. The data are reported as the means ± S.E. of the mean (n = 5 islets).

response of LipDH and ETF are contained in the observed fluorescence changes. The remaining fluorescence contributes to the base-line intensity. Although this base line complicates calculation of absolute flavoprotein concentrations, it does not affect interpretation of changes in redox potential caused by LipDH and ETF.

Redox-associated Flavin Autofluorescence Changes—We examined the 458:488 nm intensity ratio as a means of isolating the LipDH response from ETF. LipDH has a red-shifted excitation spectrum in comparison with free flavins and ETF (31). Previous work has used this red shift to partially isolate LipDH fluorescence using 488-nm excitation (17–20). Fig. 4 summarizes data collected from living pancreatic islets that were treated, as in Fig. 3, to reduce LipDH then ETF. LipDH reduction caused a ~2.5-fold increase in NAD(P)H autofluorescence (Fig. 4, *black bars*). Because of a larger contribution from mitochondria NAD(P)H intensity, this change is largely due to mitochondrial redox change with a smaller contribution from cytoplasmic regions. LipDH reduction also decreased the fluorescence observed using 458- (~10%, *black bar*) and 488-nm (~30%, *black bar*) excitations, resulting in a ~1.3-fold increase in the 458:488-nm intensity ratio. These changes are consistent with a flavoprotein response and specifically consistent with LipDH fluorescence that is in direct redox equilibrium with mitochondrial NADH (14, 15). NAD(P)H fluorescence did not change significantly with subsequent ETF reduction (Fig. 4, *black versus hatched bars*). This is due to the previous inhibition of complex I (rotenone) during LipDH reduction. This result is consistent with the NAD(P)H signal predominantly being mitochondrial in origin. Both the 458- and 488-nm image intensities lowered after ETF reduction, although these changes were small in comparison with the changes observed during LipDH reduction. In fact, the fluorescence from 458- and 488-nm images decreased only a further ~11 and ~8%, respectively. A large fraction of the autofluorescence remained in the 458- and 488-nm images consistent with significant contribution from free flavins. Because ETF reduction caused similarly small changes in the 458- and 488-nm images, the 458:488-nm intensity ratio was unaffected by this reduction. Therefore, the redox-dependent response is mainly associated with LipDH, but isolation of the LipDH response can be best achieved using a ratio of the 458- and 488-nm intensities.

To further confirm that the changes observed in the 458- and 488-nm intensities were due specifically to LipDH and ETF rather than other flavoproteins, we examined the autofluorescence changes caused by 5-min treatments of diamide (0.5 mM, n = 5) or dithiothreitol (1 mM, n = 10). These treatments nonspecifically oxidize and reduce thiols, respectively, which lead to oxidation and reduction of flavoproteins linked to the maintenance of glutathione levels. Although dithiothreitol slightly raised the 458- and 488-nm autofluorescence (1.14 ± 0.05 and 1.20 ± 0.06), neither treatment raised the relative 458:488 nm intensity ratio (0.99 ± 0.04 and 0.96 ± 0.01 for diamide and dithiothreitol, respectively). The increase in intensity observed with dithiothreitol treatment was observed only in the dim redox-responsive regions but not in the bright nonresponding regions of the 458- and 488-nm images. These results provide further evidence that the changes observed are specific to LipDH and ETF.

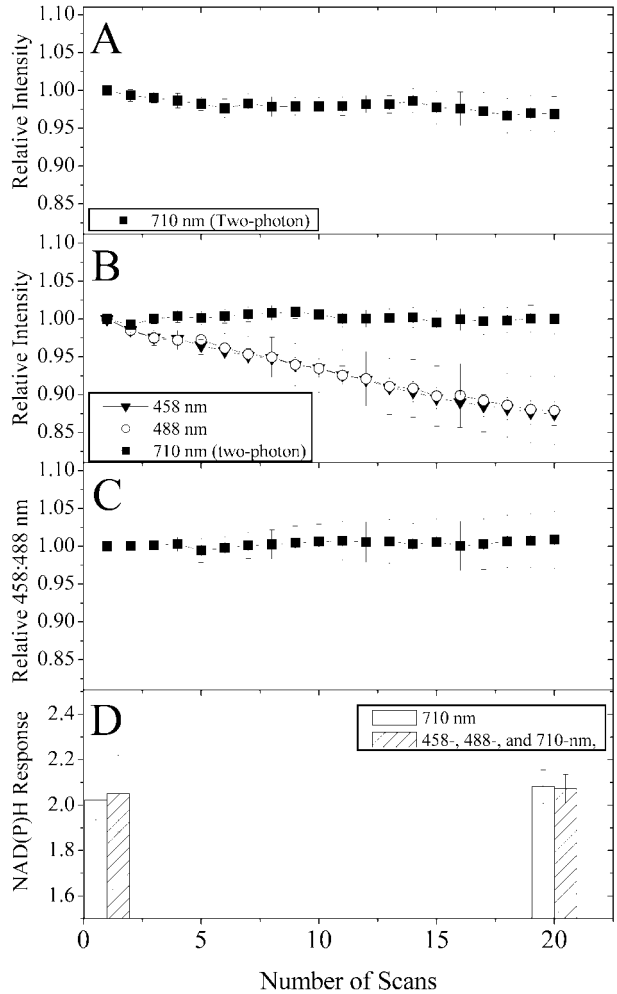

FIG. 5. **Photobleaching and phototoxicity induced by fluorescence imaging.** The islets were equilibrated in 2 mM glucose prior to imaging. *A*, the intensity collected using 710-nm excitation (n = 6). *B*, the intensity collected from sequential 458-, 488-, and 710-nm illumination (n = 8). *C*, the relative 458:488-nm intensity ratio calculated from the data collected in *B*. *D*, the glucose-induced NAD(P)H response after 1 and 20 scans of either 710 nm (*open bars*) or 458, 488, and 710 nm (*hatched bars*) (n = 3).

Phototoxicity of Illumination—Two-photon NAD(P)H imaging causes minimal phototoxicity at 710 nm with ~3 mW of laser power (1, 24). To determine whether 458- and 488-nm illumination in combination with NAD(P)H two-photon imaging is conducive to live cell imaging, we measured the photobleaching and phototoxicity induced by this method (Fig. 5). Shown in Fig. 5 are the photobleach curves and glucose-in-

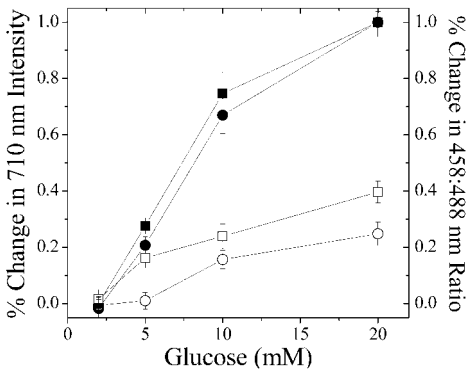

FIG. 6. **Glucose dose response of NAD(P)H and the 458:488 nm intensity ratio.** The islets were equilibrated in imaging buffer at 2 mM glucose. The NAD(P)H response (*left axis*, ■ and □) and 458:488-nm intensity ratio (*right axis*, ● and ○) are reported as the percentage of change. The islets were equilibrated in 2 mM glucose prior to 5 min of stimulation with 2, 5, 10, or 20 mM glucose (■ and ●). These islets were then treated with 2 μM FCCP and 20 mM mannoheptulose for 2 min (□ and ○). The values are reported as the averages ± the standard error of the mean. The numbers of islets measured before and after treatment were 17 and 12 for 2 mM glucose, 29 and 21 for 5 mM glucose, 26 and 18 for 10 mM glucose, and 30 and 19 for 20 mM glucose. The maximum change at 20 mM glucose resulted in an ~180 μM increase in NAD(P)H (change in 710-nm image intensity) and an ~750 nM decrease in oxidized LipDH (change in 488-nm image intensity).

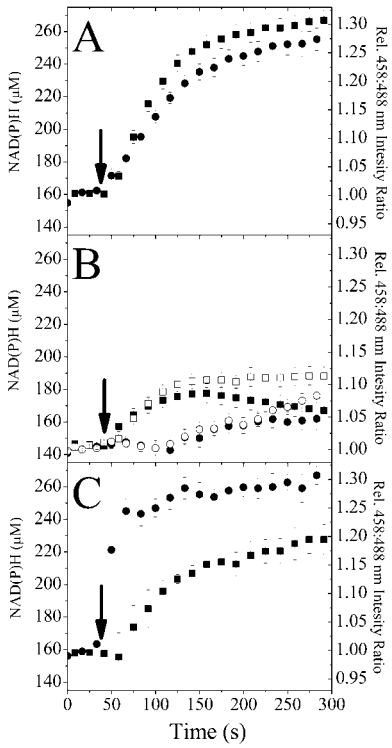

FIG. 7. **NAD(P)H and mitochondrial NADH responses to glucose, pyruvate, and methyl pyruvate.** The NAD(P)H (*left axis*, *squares*) and relative 458:488-nm intensity ratio (*right axis*, *circles*) responses with boluses of glucose, pyruvate, and methylpyruvate after the third image as indicated with *arrows*. *A*, islets were equilibrated in 2 mM glucose prior to stimulation with 20 mM glucose ($n = 10$). *B*, islets were equilibrated in 0 (■ and ●, $n = 9$) or 2 mM (□ and ○, $n = 9$) glucose prior to stimulation with 20 mM pyruvate. *C*, islets were equilibrated in 2 mM glucose prior to stimulation with 10 mM methyl pyruvate ($n = 4$).

duced NAD(P)H responses of images collected using either 710-nm excitation or sequential 458-, 488-, and 710-nm excitation. The intensity was constant from images collected using only 710-nm illumination (Fig. 5*A*). The intensity from the 710-nm excited images was also constant during sequential image collection, but the intensity from the 458- and 488-nm images decreased significantly with subsequent image collection (Fig. 5*B*). In contrast, the 458:488-nm intensity ratio remained relatively constant (Fig. 5*C*). These data indicate that confocal microscopy induces some photobleaching. The islets had a normal glucose-induced NAD(P)H response for at least 20 image collections with 710 nm or sequential 458-, 488-, and 710-nm illumination (Fig. 5*D*). This sustained glucose-response indicates minimal phototoxicity induced by the sequential scanning of the 458-, 488-, and 710-nm laser lines. Therefore, this method is conducive to live cell imaging.

Glucose Dose Response—We examined the NAD(P)H and LipDH (458:488-nm intensity ratio) glucose dose responses to determine whether NADH and NADPH are produced in a dose-dependent manner. Fig. 6 shows the relative NAD(P)H and 458:488-nm intensity ratio responses to varying amounts of glucose (Fig. 6, *closed symbols*). These curves have similar half-maximums of ~7.5 mM, which closely resembles the reported K_m for glucokinase, the rate-limiting enzyme of the β-cell glycolysis (32). These same islets were treated with 2 μM FCCP and 20 mM mannoheptulose (Fig. 6, *open symbols*). This treatment dissipates the mitochondrial proton gradient (FCCP) while blocking NADH generation in the cytoplasm through glucokinase (mannoheptulose) and results in increased NADH oxidation by the ETC. This treatment is not likely to remove NADH because transhydrogenases maintain equilibrium between mitochondrial NADH and NADPH levels. Rather, it is likely to perturb this equilibrium in favor of NADPH. This treatment lowered NAD(P)H and the 458:488-nm ratio corresponding to a decrease in the cellular redox potential. However, these curves no longer mirror each other as they did prior to treatment, and the 458:488-nm intensity ratio was lowered to a greater extent than NAD(P)H. These data are consistent with biochemical evidence that glucose metabolism causes a build-up of both NADH and NADPH in β-cells (33). A difference in the responses is only observed when the islet is pushed to preferentially utilize NADH.

Temporal Glucose- and Pyruvate-induced Responses—We examined the temporal separation of the NADH and NADPH responses during glucose, pyruvate, and methyl pyruvate stimulation. Shown in Fig. 7 are the temporal NAD(P)H and LipDH (relative 458:488-nm intensity ratio) responses to these metabolites. Glucose stimulation caused a rapid rise in NAD(P)H with a similarly shaped LipDH response (Fig. 7*A*). These data are consistent with a concurrent rise in NADH and NADPH. Islets were also equilibrated with 0 (*closed symbols*) or 2 mM (*open symbols*) glucose prior to the addition of 20 mM pyruvate (Fig. 7*B*). This amount of glucose is nonstimulatory but provides the islet with a small amount of glycolysis through hexokinase metabolism. The addition of pyruvate in the absence of glucose caused a transient rise in NAD(P)H (Fig. 7*B*, ■). In contrast, the response with glucose present was stable for at least 300 s (□). In the absence or presence of glucose, there was little change in the pyruvate-induced LipDH response at early time points (● and ○). These responses slowly increased after 100 s but never reached the levels observed during glucose stimulation. It is likely that the slow increase observed is due to re-establishment of the equilibrium between NADH and NADPH levels through transhydrogenase. At later time points (>250 s), the LipDH response was larger in the presence than in the absence of glucose. It should also be noted that the changes in intensity occurred uniformly between cells, consistent with this response being a β-cell rather than non-β-cell response. These data indicate that pyruvate initially stimulates a significant NADPH response in the absence of NADH. The NADH response, as indicated by LipDH, increased with

further metabolism. This increase was accompanied by a decrease in NADPH unless nonstimulatory glucose was present. Therefore, the pyruvate-stimulated NAD(P)H response is kinetically separated into a NADPH rise followed by a small NADH response. The final response of NADH and NADPH is enhanced by the presence of nonstimulatory glucose.

Methyl pyruvate has been shown to induce insulin secretion, presumably by increased transport into β-cells where it is then hydrolyzed to pyruvate. However, methyl pyruvate has been reported to stimulate insulin secretion directly through ATP-sensitive K^+ channels and not cause a significant rise in NAD(P)H intensity (34). This metabolite also causes less lactate production, which is consistent with decreased cytoplasmic metabolism and increased mitochondrial metabolism (35). The addition of methyl pyruvate caused larger and sustained NAD(P)H (■) and LipDH (●) responses (Fig. 7*C*). This response was faster than that observed with glucose or pyruvate. These data are consistent with stimulation of both NADPH and NADH. These data are also inconsistent with a direct affect of methyl pyruvate on ATP-sensitive K^+-channels, because such an affect would limit the NAD(P)H response.

DISCUSSION

We have shown previously that exogenous pyruvate causes a transient rise in β-cell mitochondrial NAD(P)H (3). To separate the responses of NADH and NADPH, we now compare the pyruvate-stimulated NAD(P)H response to that of LipDH flavoprotein, which is in redox equilibrium with mitochondrial NADH. To measure the LipDH response, flavin autofluorescence was imaged quantitatively by confocal microscopy. We examined the fluorescence contributions from the two predominant redox-responsive flavoproteins, LipDH and ETF, using inhibitors to complex I and III of the ETC. A large portion of intensity remained after the reduction of both LipDH and ETF, which indicated a significant contribution from free flavins to the observed fluorescence (19, 20). A significant LipDH fluorescence response was observed using 488-nm confocal imaging, but a distinct measure could not be made using a single excitation wavelength because of ETF contamination. In contrast, the 458:488-nm intensity ratio significantly increased during LipDH reduction but was unaffected by ETF reduction. These studies showed no evidence for intensity changes because of flavoproteins other than LipDH and ETF. Collection of the 458- and 488-nm images induced some photobleaching, but the islets maintained normal glucose responsiveness for the period of study. Therefore, we used the 458:488-nm intensity ratio to isolate the LipDH response and obtained an independent measure of mitochondrial NADH for comparison with the NAD(P)H signal.

We compared the NAD(P)H and LipDH responses during pancreatic islet metabolite stimulation to assay NADH and NADPH production. This yields information regarding the likely routes of pyruvate metabolism, because NADH and NADPH are likely dependent on PDH and PC metabolism, respectively. The NAD(P)H and LipDH glucose dose responses were similar prior to FCCP and mannoheptulose treatment (Fig. 6). This treatment enhances the use of NADH by the ETC making the signal from NADPH proportionally larger. We observed a smaller LipDH response than NAD(P)H after treatment, indicating that the NAD(P)H response prior to treatment was due to both NADH and NADPH. Further, the glucose-stimulated NADH and NADPH responses were kinetically inseparable (Fig. 7*A*). The pyruvate-stimulated response was initially dominated by NAD(P)H followed by a slow increase in LipDH. In the absence of glucose, the rise in LipDH was accompanied by a fall in NAD(P)H. In contrast, the NAD(P)H response was stable, and the final LipDH response was increased in the presence of nonstimulatory glucose. These data indicate that exogenous pyruvate initially stimulates a rise in NADPH that is followed by a slow rise in mitochondrial NADH. As the NADH response increases during pyruvate stimulation, the total NAD(P)H signal falls. Nonstimulatory glucose inhibits this fall and enhances the final mitochondrial NADH response. We previously showed that cytoplasmic regions respond to pyruvate with a sustained rise in NAD(P)H intensity (3). This sustained NAD(P)H response was modeled to include NADPH production through pyruvate-cycling (3), but the generation of this signal can also be due to isocitrate leaving the mitochondria for NADPH production through isocitrate dehydrogenase. Furthermore, it is likely that a fraction of the NADPH response is localized to mitochondria. A likely candidate for the production of this NADPH is mitochondrial $NADP^+$-dependent isocitrate dehydrogenase. Methyl pyruvate is a known insulin secretagogue that is thought to diffuse into the β-cell at a faster rate than exogenous pyruvate. Once inside the cell, methyl pyruvate is thought to be hydrolyzed and supplied to the mitochondria. We observed a significant and immediate response in NAD(P)H and LipDH to methyl pyruvate (Fig. 7*C*). These data are consistent with glycolytic pyruvate and methyl pyruvate being metabolized through PC and PDH, with exogenous pyruvate preferentially stimulating NADPH, likely through PC metabolism.

Our data indicate that exogenous pyruvate fails to induce a sustained mitochondrial NADH response. This failure to stimulate a sustained NADH response likely limits the production of ATP for stimulated insulin secretion. The inability of exogenous pyruvate to stimulate a NADH response may be due to inactivity of PDH or other tricarboxylic acid cycle enzymes. It has been proposed that the β-cell tricarboxylic acid cycle needs to be primed with calcium influx to metabolize pyruvate (36). However, we have shown before that the mitochondrial NAD(P)H response is fully active during glucose stimulation prior to calcium influx (2, 3). Therefore, we believe that the β-cell tricarboxylic acid cycle is active and will metabolize pyruvate in the absence of a priming event.

Because the tricarboxylic acid cycle is active, the inability of exogenous pyruvate to stimulate a sustained mitochondrial NADH response is likely due to either limited supply of substrate to PDH or loss of the resulting NADH response by other means. β-Cell metabolism has previously been modeled to metabolically compartmentalize pyruvate (11). This model indicates that glycolysis supplies PDH and PC metabolism through two independent pyruvate pools that minimally interact (11). Interpreted within this model, our data on glucose stimulation are consistent with a supply of pyruvate to both pools. In contrast, pyruvate initially stimulates only NADPH, suggesting a preferential supply of pyruvate to the PC pool and limited supply to the PDH pool. Pyruvate compartmentalization has been observed previously in perfused rat heart (37). Similar to our studies, rat heart has one pyruvate pool that closely couples to the glycolytic system and a second pool that closely couples to extracellular pyruvate. This would mean that the NADH response will increase with a facilitated supply of exogenous pyruvate to PDH. Consistent with this possibility, we observed a larger NADH and NADPH response with methyl pyruvate than with pyruvate. It has also been shown that overexpression of membrane monocarboxylate transporter-1 in rat pancreatic islets enabled pyruvate-stimulated insulin secretion (38). Thus far, however, the mechanism behind pyruvate compartmentalization remains unclear.

Our data can also be modeled to include NADH production through PDH-dependent tricarboxylic acid cycle metabolism in parallel with another route that utilizes NADH. These compet-

ing mechanisms result in no net NADH increase. Although β-cells are reported to have low lactate dehydrogenase activity, we have previously detected lactate production from pancreatic islets during exogenous pyruvate stimulation (3). The lowering of cytoplasmic NADH reduces availability for shuttling into mitochondria. Furthermore, mitochondrial redox potential is likely lowered in the β-cell because of PC-dependent production of oxaloacetate. A build-up of oxaloacetate promotes malate production and lowered mitochondrial NADH. It is unlikely that malate was metabolized to pyruvate (producing NADPH) because mouse islets show low malic enzyme activity (13). In contrast to exogenous pyruvate, glucose metabolism maintains cytoplasmic NADH production through glycolysis. Our data with exogenous pyruvate stimulation in the presence of 0 or 2 mM glucose is in agreement with this assessment, because 2 mM glucose increased the later time point mitochondrial NADH levels (Fig. 7*B*). In contrast to exogenous pyruvate, fast methyl pyruvate transport likely increases the availability of pyruvate to PDH. Also, methyl pyruvate has been shown to cause less lactate production than pyruvate (35), consistent with its being less metabolized in the cytoplasm than exogenous pyruvate.

In summary, our data indicate that exogenous pyruvate stimulates a transient rise in NADPH in the absence of a significant NADH response. We have modeled this to be due to either limited supply of substrate to PDH dependent metabolism or a buffering of the NADH response caused by redox lowering mechanisms.

Acknowledgment—We thank Owen McGuinness for helpful discussion.

REFERENCES

1. Bennett, B. D., Jetton, T. L., Ying, G., Magnuson, M. A., and Piston, D. W. (1996) *J. Biol. Chem.* **271,** 3647–3651
2. Patterson, G. H., Knobel, S. M., Arkhammar, P., Thastrup, O., and Piston, D. W. (2000) *Proc. Natl. Acad. Sci. U. S. A.* **97,** 5203–5207
3. Rocheleau, J. V., Head, W. S., Nicholson, W. E., Powers, A. C., and Piston, D. W. (2002) *J. Biol. Chem.* **277,** 30914–30920
4. Newgard, C. B., and McGarry, J. D. (1995) *Annu. Rev. Biochem.* **64,** 689–719
5. MacDonald, M. J. (1995) *J. Biol. Chem.* **270,** 20051–20058
6. Corkey, B. E., Glennon, M. C., Chen, K. S., Deeney, J. T., Matschinsky, F. M., and Prentki, M. (1989) *J. Biol. Chem.* **264,** 21608–21612
7. Brun, T., Roche, E., Assimacopoulos-Jeannet, F., Corkey, B. E., Kim, K. H., and Prentki, M. (1996) *Diabetes* **45,** 190–198
8. MacDonald, M. J. (1993) *Metabolism* **42,** 1229–1231
9. Khan, A., Ling, Z. C., and Landau, B. R. (1996) *J. Biol. Chem.* **271,** 2539–2542
10. Schuit, F., De Vos, A., Farfari, S., Moens, K., Pipeleers, D., Brun, T., and Prentki, M. (1997) *J. Biol. Chem.* **272,** 18572–18579
11. Lu, D., Mulder, H., Zhao, P., Burgess, S. C., Jensen, M. V., Kamzolova, S., Newgard, C. B., and Sherry, A. D. (2002) *Proc. Natl. Acad. Sci. U. S. A.* **99,** 2708–2713
12. Farfari, S., Schulz, V., Corkey, B., and Prentki, M. (2000) *Diabetes* **49,** 718–726
13. MacDonald, M. J. (2002) *Am. J. Physiol.* **283,** E302–E310
14. Hassinen, I., and Chance, B. (1968) *Biochem. Biophys. Res. Commun.* **31,** 895–900
15. Chance, B., Schoener, B., Oshino, R., Itshak, F., and Nakase, Y. (1979) *J. Biol. Chem.* **254,** 4764–4771
16. Wagnieres, G. A., Star, W. M., and Wilson, B. C. (1998) *Photochem. Photobiol.* **68,** 603–632
17. Kunz, W. S., and Kunz, W. (1985) *Biochim. Biophys. Acta* **841,** 237–246
18. Voltti, H., and Hassinen, I. E. (1978) *J. Bioenerg. Biomembr.* **10,** 45–58
19. Kunz, W. S., and Gellerich, F. N. (1993) *Biochem. Med. Metab. Biol.* **50,** 103–110
20. Kunz, W. S. (1986) *FEBS Lett.* **195,** 92–96
21. Huang, S., Heikal, A. A., and Webb, W. W. (2002) *Biophys. J.* **82,** 2811–2825
22. Scharp, D. W., Kemp, C. B., Knight, M. J., Ballinger, W. F., and Lacy, P. E. (1973) *Transplantation* **16,** 686–689
23. Stefan, Y., Meda, P., Neufeld, M., and Orci, L. (1987) *J. Clin. Invest.* **80,** 175–183
24. Piston, D. W., and Knobel, S. M. (1999) *Methods Enzymol.* **307,** 351–368
25. Arkhammar, P. O. G., Bernard, R. Kofod, T. H., and Thastrup, O. (1998) *Methods Cell Sci.* **19,** 255–268
26. Piston, D. W., Patterson, G. H., and Knobel, S. M. (1999) *Methods Cell Biol.* **58,** 31–48
27. Patel, M. S., Vettakkorumakankav, N. N., and Liu, T.-C. (1995) *Methods Enzymol.* **252,** 186–195
28. Zhang, Q., Piston, D. W., and Goodman, R. H. (2002) *Science* **295,** 1895–1897
29. Brunk, U. T., and Terman, A. (2002) *Free Radic. Biol. Med.* **33,** 611–619
30. Hall, C. L., and Kamin, H. (1975) *J. Biol. Chem.* **250,** 3476–3486
31. Maeda-Yorita, K., and Aki, K. (1984) *J. Biochem.* (*Tokyo*) **96,** 683–690
32. Matschinsky, F. M., Glaser, B., and Magnuson, M. A. (1998) *Diabetes* **47,** 307–315
33. Ramirez, R., Rasschaert, J., Sener, A., and Malaisse, W. J. (1996) *Biochim. Biophys. Acta* **1273,** 263–267
34. Dufer, M., Krippeit-Drews, P., Buntinas, L., Siemen, D., and Drews, G. (2002) *Biochem. J.* **368,** 817–825
35. Malaisse, W. J., Jijakli, H., Ulusoy, S., Cook, L., Best, L., Vinambres, C., Villanueva-Penacarrillo, M. L., Valverde, I., and Sener, A. (1996) *Arch. Biochem. Biophys.* **335,** 229–244
36. Eto, K., Tsubamoto, Y., Terauchi, Y., Sugiyama, T., Kishimoto, T., Takahashi, N., Yamauchi, N., Kubota, N., Murayama, S., Aizawa, T., Akanuma, Y., Aizawa, S., Kasai, H., Yazaki, Y., and Kadowaki, T. (1999) *Science* **283,** 981–985
37. Peuhkurinen, K. J., Hiltunen, J. K., and Hassinen, I. E. (1983) *Biochem. J.* **210,** 193–198
38. Ishihara, H., Wang, H., Drewes, L. R., and Wollheim, C. B. (1999) *J. Clin. Invest.* **104,** 1621–1629